Supplementary information for

Compressive hyperspectral phasor imaging with single-pixel detection for spectral tasks

Jiaqi Song[1,4], Baolei Liu [2,3,*], Muchen Zhu[1], Yao Wang[1], Yue Yu[2], Zhaohua Yang[2,3], Xiaolan Zhong[1], Fan Wang[1,*]

[1] School of Physics, Beihang University, Beijing 100191, China

[2] School of Instrumentation Science and Optoelectronic Engineering, Beihang University, Beijing 100191, China

[3] Hangzhou International Innovation Institute, Beihang University, Hangzhou, 311115, China

[4] Institute of Physics, China Academy of Sciences, Beijing 100190, China

These authors contributed equally to this work: Jiaqi Song and Baolei Liu

* Correspondence: liubaolei@buaa.edu.cn, fanwang@buaa.edu.cn

Table of Contents

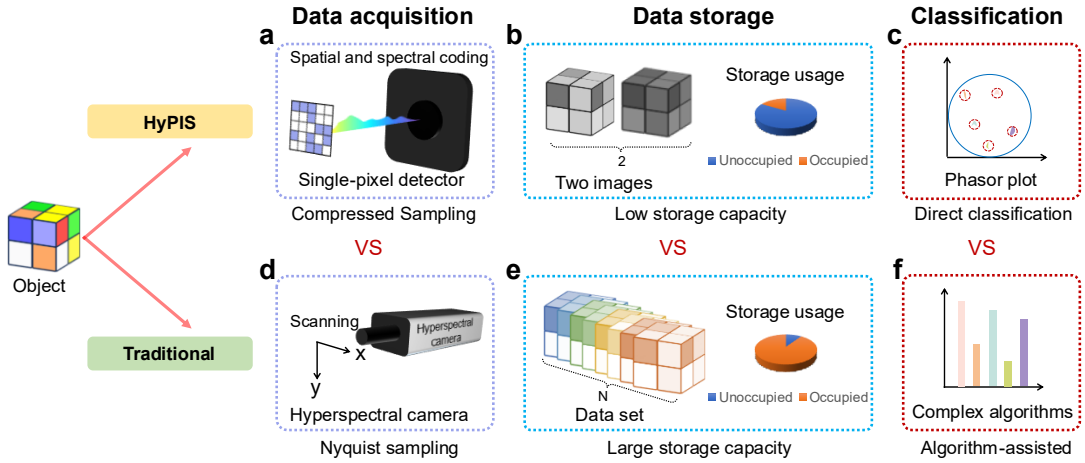

Fig. S1. Comparison between HyPIS and the traditional method in the hyperspectral image classification process. a, The data acquisition process of HyPIS. **b,** The data storage capacity of HyPIS. **c,** The classification of HyPIS. **d,** The data acquisition process of traditional methods. **e,** The data storage capacity of traditional methods. **f,** The classification of traditional methods.

Figure S1 presents a systematic comparison between the HyPIS and the traditional strategies in the complete workflow of hyperspectral image classification, including three key steps: data acquisition, data storage, and classification. Specifically, in the data acquisition stage (Figs. S1a and S1d), HyPIS achieves compressed sampling through spatial-spectral encoding and collects target information using a single-pixel detector (SPD). In contrast, traditional methods rely on hyperspectral cameras for spatially scanning, which follows the Nyquist sampling criterion. For data storage (Figs. S1b and S1e), HyPIS demonstrates that it only requires storing two images, resulting in low memory usage (as can be seen from the large unused portion in the memory pie chart). In contrast, traditional methods need to store large datasets, leading to significantly increased storage requirements and high memory usage. Moreover, in the classification stage (Figs. S1c and S1f), HyPIS achieves direct classification through phasor plot, simplifying the workflow without relying on complex post-processing. In contrast, traditional methods require deploying complex algorithms to support classification, which adds additional computational complexity. In summary, compared to traditional hyperspectral image classification methods, these comparative analyses collectively highlight the core advantages of HyPIS, including efficient data acquisition, reduced storage burden, and simplified hyperspectral image classification.

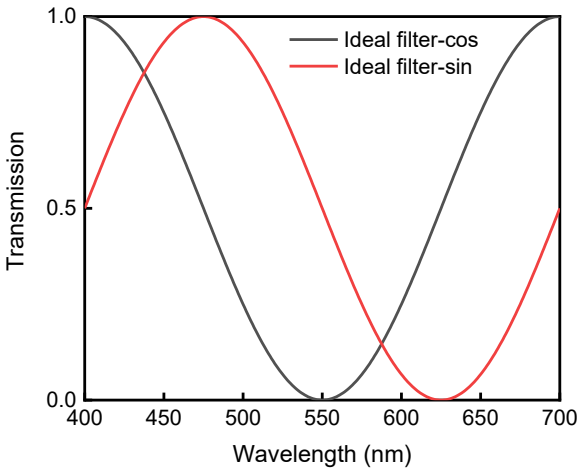

Fig. S2. Transmittance spectra of ideal filter-cos and ideal filter-sin used in the simulation.

In order to ensure consistency with the spectral range of the public datasets, we simulate a set of sine and cosine filters operating in the 400-700 nm wavelength range, as shown in Fig. S2, in which the red line represents the ideal filter-sin and the black line represents the ideal-cos.

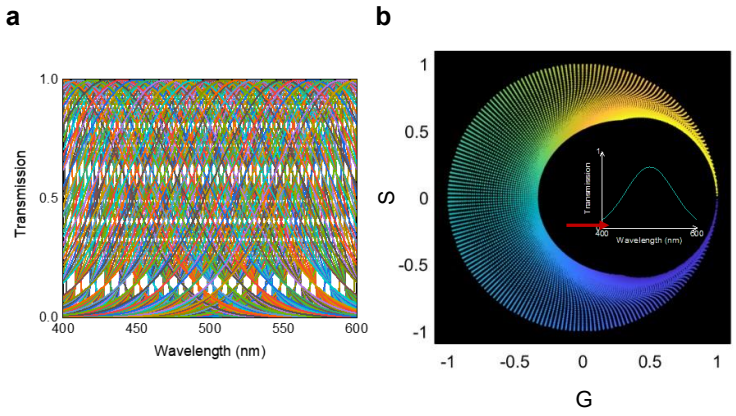

Fig. S3. Simulated spectra and their corresponding phasor representations. a, Simulated spectra. **b,** ideal phasor plot.

As described in the main text, any spectral curve can be represented as a point in the phasor plot shown in Fig. 3i of the main text. We simulated a set of Gaussian spectra in the 400–600 nm range, with center wavelengths ranging from 400 nm to 600 nm in 1 nm intervals, and full width at half maximum (FWHM) ranging from 2 nm to 100 nm in 2 nm intervals. Figure S3a shows these spectral curves. Using the ideal filters from Fig. S2, combined with the conventional Phasor algorithm, the G and S values of these spectra were calculated. It can be observed that these spectra can all be encoded into the phasor plot determined by the ideal two filters, as shown in the results in Fig. S3b.

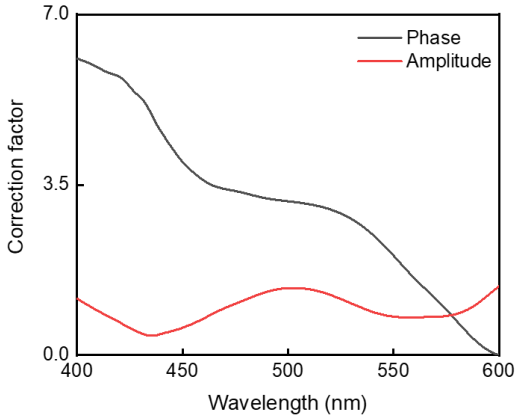

Fig. S4. Calibration factors of phase and amplitude.

Obtaining ideal filter-cos and ideal filter-sin is difficult, requiring special design and processing. To present a low-cost solution, in the experiment we used inexpensive color filters. Through post-processing corrections, these filters can have the same modulation scheme as the ideal filter-cos and ideal filter-sin within the wavelength range of 400-600 nm. Figure S4 shows the calibration factors of phase and amplitude.

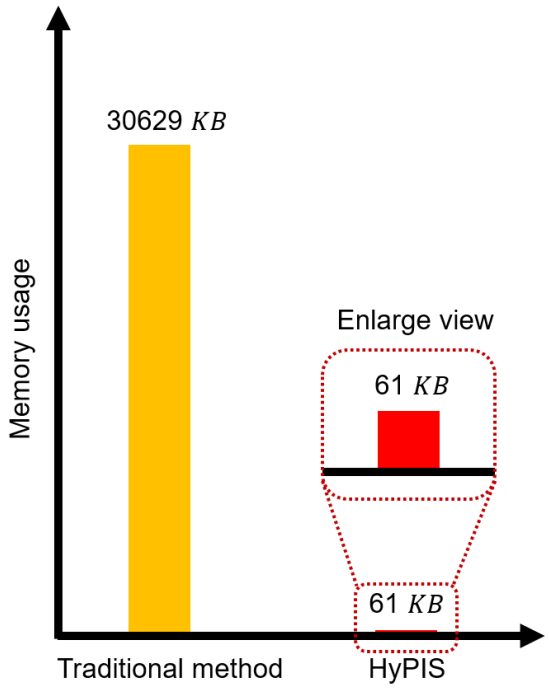

Fig. S5. Comparison of memory usage between traditional methods and HyPIS during the classification process.

To compare the memory usage of HyPIS with the traditional hyperspectral classification method, we used a simplified method to construct a hyperspectral dataset that can achieve the same classification results as HyPIS. As described in the main text of Fig. 4H(i), we first collected spectra from different regions of clover using a spectrometer, then assigned these spectra to grayscale images reconstructed from single pixels, ultimately obtaining a 3D hyperspectral data cube. We then compared the memory usage of the two schemes. As shown in Figure S5, it can be seen that the traditional scheme requires about 30,629 KB of memory, whereas HyPIS only requires 61 KB, representing a 500-fold reduction in memory usage.

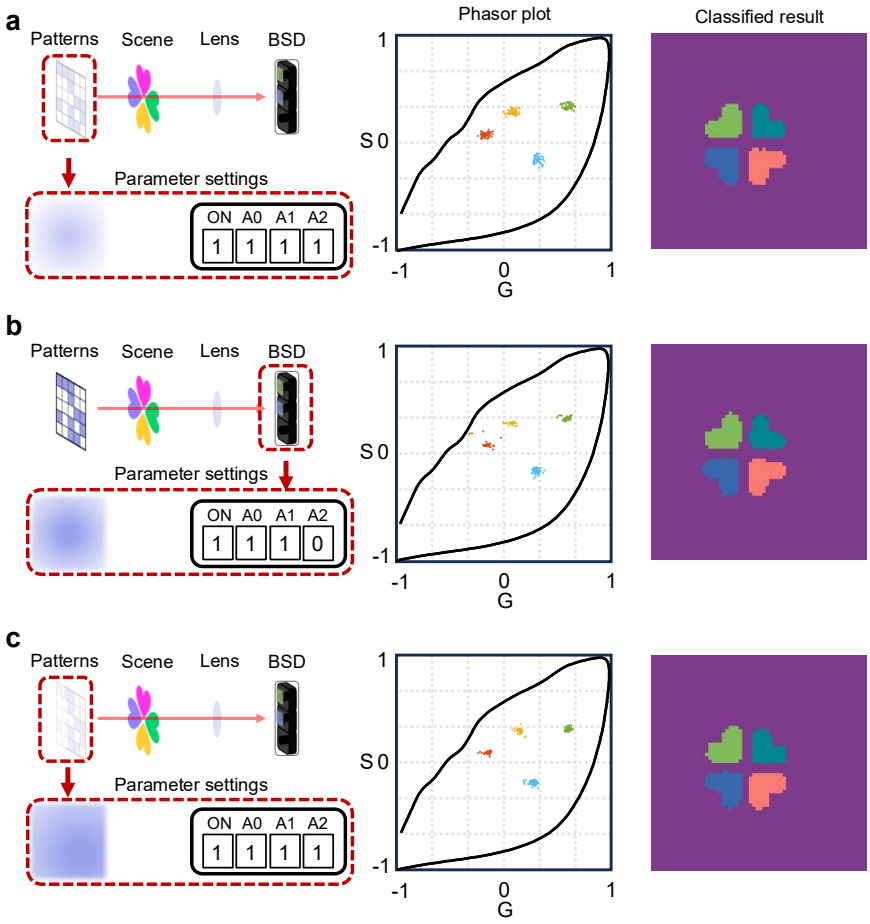

Fig. S6 HyPIS for hyperspectral phasor imaging and classification under different light distribution and detector gains. The first column shows different experimental conditions, the second column shows the reconstructed two-dimensional phasor plots, and the third column shows the classification results. The results in Fig. 4d in the main text serve as the control group. **a**, Illumination intensity was set to a lower level than the control group, and the detector gain is 70 dB. **b**, Distribution of the illumination light field remained identical to that of the control group, while the detector gain was decreased to 40 dB. **c**, Illumination field intensity distribution exhibited a non-Gaussian light distribution, and the detector gain was set at 70 dB.

To verify the robustness of HyPIS performance in hyperspectral image classification, we conducted experiments under different lighting conditions and detector gains. The result in Fig. 4 in the main text is set as the control group, which utilized a detector gain of 70 dB and a quasi-uniform light distribution with strong illumination. We then investigated the performance of HyPIS under three different conditions of illumination and detector gains. As denoted by the red dashed in the first column of Fig. S6, the three conditions are: (a) the illumination intensity was set at a lower level than that of the control group while keeps the same light field distribution, while the detector gain was maintained at 70 dB that is same to the control group; (b) the illumination light field remained identical to that of the control group, while the detector gain was decreased to 40 dB; (c) the illumination light field exhibited a non-uniform Gaussian distribution, and the detector gain was set at 70 dB. Though there are slightly different point distributions, the general phasor representations (the second column in Fig. S6) and the classification result images (the third column

in Fig. S6) keep the similar distributions with the reference in Fig. 4f in main text. The results indicate that the results of HyPIS are unaffected by the illumination distribution of the light source used, whether it is Gaussian or non-Gaussian, nor by the gain of the detector. Instead, they are exclusively contingent upon the intrinsic spectral characteristics of the objects themselves.

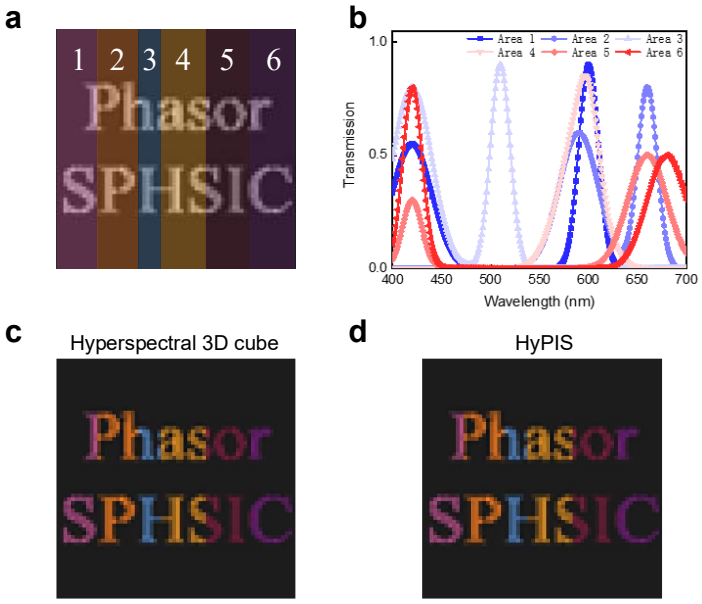

Fig. S7. Simulated results of a color image reconstructed using HyPIS. a, Image used in the simulation, where 6 regions on the image have different spectral curves. **b,** Spectral response curves of the 6 regions. **c,** Color of the image reconstructed from 3D hyperspectral data. **d,** Color of the image reconstructed using HyPIS.

Modern RGB color cameras can classify scenes by capturing the color and spatial information of objects. However, the effectiveness of this classification is inherently limited by the spectral response characteristics of the red, green, and blue channels in these cameras. In a color camera, the grayscale image captured by each channel corresponds to the combined intensity of the object passed through the red, green, and blue filters. These three images are then linearly combined to reconstruct the color image. As for HyPIS, it uses phasor analysis to process spectral information and SPI to handle spatial information, thereby achieving high-fidelity spatial-spectral information processing. Therefore, HyPIS can not only perform hyperspectral image classification but also reconstruct high-quality full-color images of target objects. We first demonstrated this capability of HyPIS through simulations.

Figure S7 shows the simulation results of color images reconstructed using HyPIS. The original image used for the simulation is shown in Fig. S7a, which is divided into six different regions (labeled 1–6), each with unique spectral characteristics. Figure S7b shows the transmission spectral response curves of the six regions in the wavelength range of 400–700 nm, providing different spectral features for each region. Figure S7c shows a color image reconstructed from hyperspectral 3D cube data, serving as a high-fidelity reference for color representation. The color image generated using the HyPIS method is shown in Fig. S7d. Simulation results indicate that the images reconstructed by HyPIS are highly consistent with the reference image (Fig. S7c) in terms of color presentation: both accurately reproduce the unique color characteristics of each labeled region in the original input image. These results confirm that HyPIS can effectively capture the intrinsic spectral characteristics of different regions and convert them into accurate color information, thereby validating its ability to perform high-quality color image reconstruction.

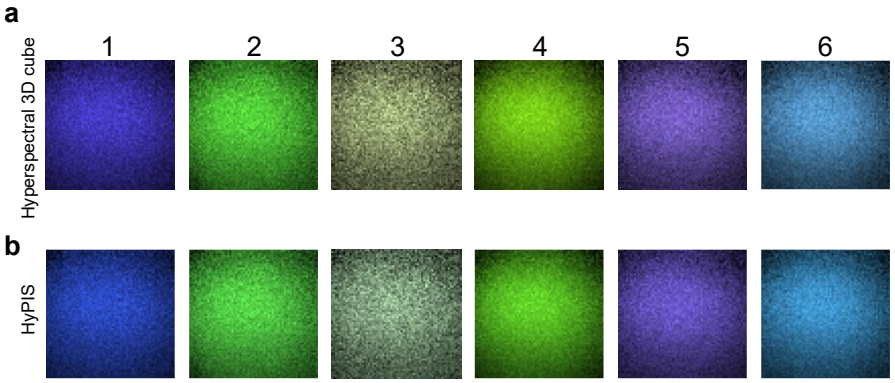

Fig. S8. Experimental results of the ColorChecker target using HyPIS. a, Color image reconstructed from hyperspectral data acquired in the experiment. **b,** Color image reconstructed using HyPIS in the experiment.

We further experimentally verified that HyPIS is capable of producing high-quality color images. Figure S8 shows the experimental color image reconstruction performance of HyPIS tested using a color calibration target. We selected six different color regions as target. Figure S8a displays the color image reconstructed from the hyperspectral data cube obtained in the experiment, with the data cube acquired in the same way as in Fig. 4h(i) in the main text. The color image reconstructed from this data serves as a high-fidelity reference, reflecting the true color characteristics of the six target areas. Figure S8b shows the color image reconstructed using the HyPIS method in the same experiment which evident that the image reconstructed by HyPIS is highly consistent with the hyperspectral reference image, validating its capability to reconstruct full-color images.

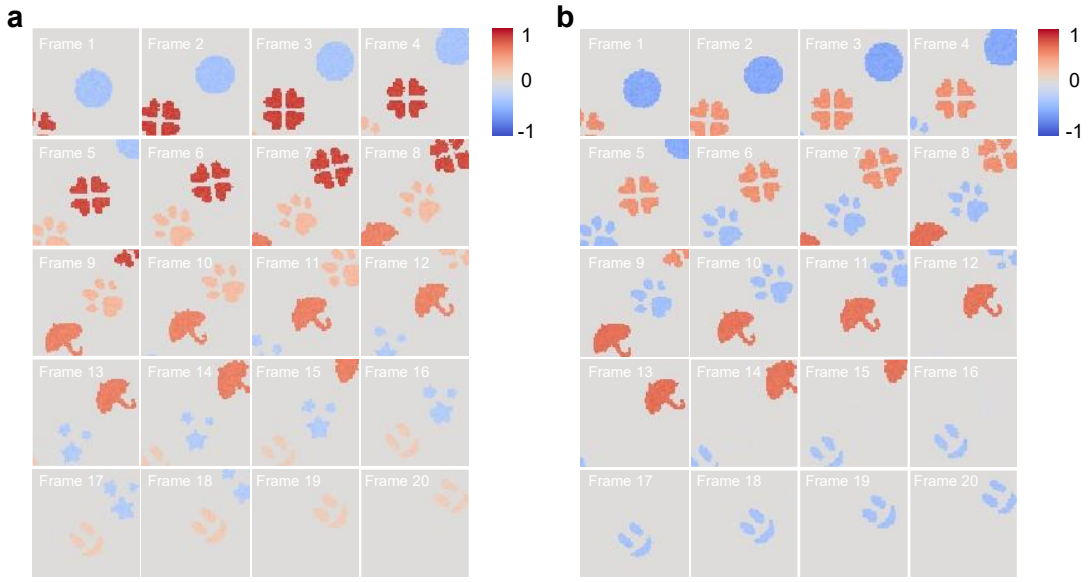

Fig. S9. The reconstructed a, G and b, S of the rotating turntable.

Figure S9 shows 20 reconstructed frames of the G and S videos corresponding to the dynamic scene reconstructed using HyPIS, with a frame rate of approximately 2.68 fps and each frame having a size of 64×64 pixels.

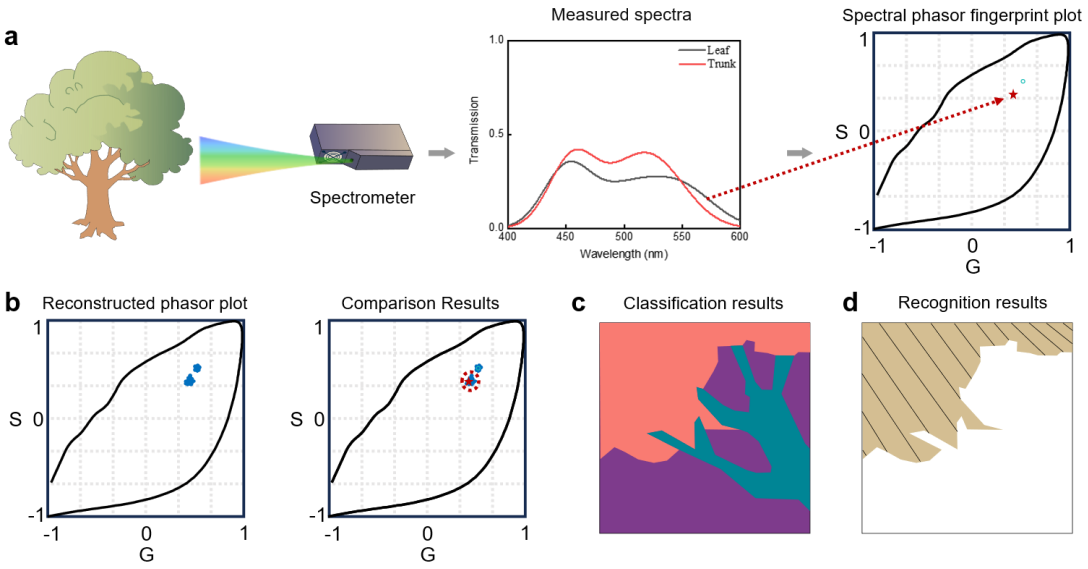

Fig. S10. Flowchart of HyPIS for hyperspectral image classification and recognition. a, Left: Acquiring the spectrum of an object using a spectrometer. Middle: Recording the spectral measurement. Right: Calculating the spectral phasor fingerprints plot. **b,** Left: Obtaining the phasor plot using traditional algorithms. Right: Comparing the results obtained from HyPIS with the left subfigure of B. **c,** Classification results. **d,** Recognition leaf area results.

HyPIS can not only directly achieve hyperspectral image classification but also recognize objects in the detected scene, which holds significant implications for the field of optical remote sensing. To demonstrate this application, we proposed a phasor diagram-based classification and recognition strategy. Figure S10 illustrates the flowchart of our proposed strategy for using HyPIS for hyperspectral image classification and recognition. First, the pre-measured spectral data of known objects are used to calculate the spectral phasor fingerprints plot via the traditional Phasor algorithm, with the results serving as the spectral phasor fingerprints plot (Fig. S10a). Then, the 2D phasor plot obtained by HyPIS is compared with the spectral phasor fingerprints plot, and points on the reconstructed 2D vector spectrogram are subjected to regional segmentation (Fig. S10b). Finally, according to the segmented results, the classification results (Fig. S10c) and recognition results (Fig. S10d) of the detected scene can be obtained.

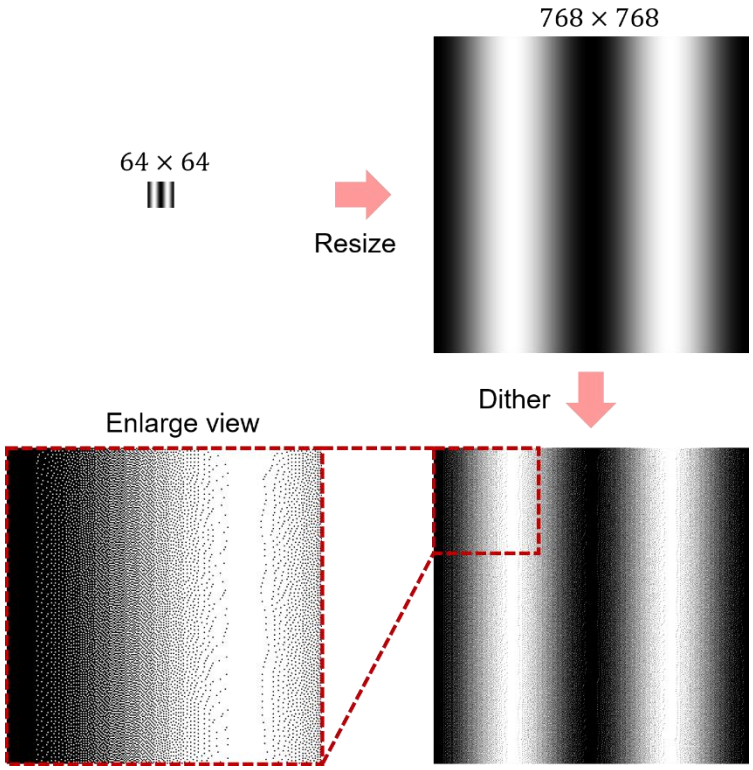

Fig. S11. Processing process of the spatial dithering method. First, a 64×64 gray-coded pattern was resized into a 768×768 grayscale pattern, and then dithered into a 768×768 binary pattern.

Figure S11 shows the step-by-step workflow of the spatial dithering method. Initially, a 64×64 grayscale encoded pattern (shown in the upper left of the figure) was resized to a 768×768 grayscale image (shown in the upper right of the figure). This enlarged image exhibits smooth grayscale gradients while retaining the spatial intensity distribution of the original 64×64 pattern. Next, dithering is applied to this 768×768 grayscale image, converting it into a 768×768 binary image (as shown in the lower right panel). The red dashed box and the corresponding enlarged view further illustrate the pixel-level details of the dithered output. Next, dithering is applied to this 768×768 grayscale image, converting it into a 768×768 binary image (as shown in the lower right corner of the figure). The red dashed box shows some detailed results of the dithered image (as shown in the lower left corner of the figure). This two-step process (scaling first and then dithering) effectively converts a small grayscale-coded pattern into a high-resolution binary image, meeting the requirements for high-precision spatial encoding in imaging systems.